Kinetics of CO_2 adsorption on cherry stone-based carbons in CO_2/CH_4 separations

N. Álvarez-Gutiérrez, M.V. Gil[†], F. Rubiera, C. Pevida*

Instituto Nacional del Carbón, INCAR-CSIC. Apartado 73, 33080 Oviedo, Spain.

[†] *Present address: Department of Chemical Engineering, Norwegian University of Science and Technology, Sem Sælands vei 4, Trondheim, NO-7491, Norway*

Abstract

Most practical applications of solids in industry involve porous materials and adsorption processes. A correct assessment of the equilibrium and kinetics of adsorption is extremely important for the design and operation of adsorption based processes. In our previous studies we focused on the evaluation of the equilibrium of CO_2/CH_4 adsorption on cherry stone-based carbons. In the present paper the kinetics of adsorption of CO_2 on two cherry stone-based activated carbons (CS-H_2O and CS-CO_2), previously prepared in our laboratory, has been evaluated by means of transient breakthrough experiments at different CO_2/CH_4 feed concentrations, at atmospheric pressure and 30 ˚C. A commercial activated carbon, Calgon BPL, has also been evaluated for reference purposes. Three models have been applied to estimate the rate parameters during the adsorption of CO_2 on these carbons, pseudo-first, pseudo-second and Avrami´s fractional order kinetic models. Avrami´s model accurately predicted the dynamic CO_2 adsorption performance of the carbons for the different feed gas compositions. To further investigate the mechanism of CO_2 adsorption on CS-H_2O, CS-CO_2 and Calgon BPL, intra-particle diffusion and Boyd´s film-diffusion models were also evaluated. It was established that mass transfer during the adsorption of CO_2 from CO_2/CH_4 is a diffusion-based process and that the main diffusion mechanisms involved

are intra-particle and film diffusion. At the initial stages of adsorption, film diffusion resistance governed the adsorption rate, whereas intra-particle diffusion resistance was the predominant factor in the following stages of adsorption.

*Corresponding author. Tel.: +34 985 119 090; Fax: +34 985 297 662

E-mail address: cpevida@incar.csic.es (C. Pevida)

Keywords: Biomass-based activated carbon; Biogas; CO_2 capture; Breakthrough test; Kinetic model

1. Introduction

Pressure swing adsorption (PSA) has become very prominent in the purification of gases for multiple applications, namely air purification [1, 2], hydrogen separation and purification [3-6], and CO_2 capture [7, 8]. Due to their ability to separate carbon dioxide from methane, PSA processes are currently being extended to areas like biogas and landfill gas upgrading. This separation technology might reduce energy consumption without the need for using toxic and corrosive chemicals as in chemical absorption [9, 10].

Many types of porous media have been developed for CO_2/CH_4 separation such as carbon molecular sieves [11], zeolites [12], metal-organic frameworks [13], and activated carbons [14]. The main PSA technology for enriching biogas in CH_4 is based on zeolites, due to their high selectivity towards CO_2. However, some interesting properties of activated carbons such as their high adsorption capacity at moderate pressure, hydrophobic character, significantly low cost compared to zeolites and

amenability to pore structure modification and surface functionalization make them highly suitable materials for gas adsorption [15]. Moreover, they can be prepared from a large variety of low cost raw materials [16-18]. Previous research conducted in our laboratory has successfully demonstrated the great potential of cherry stone-based carbons for biogas upgrading. They were tested for their CO_2 and CH_4 equilibrium adsorption capacities at high pressures under static [19] and dynamic conditions in a purpose-built lab-scale fixed-bed unit [20].

For industrial application, a promising adsorbent must exhibit not only a high CO_2 adsorption capacity and selectivity, but also a rapid adsorption rate. Such requirements make it necessary to have an adequate understanding of adsorption kinetics [21].

Currently, the literature provides a wide number of kinetic models [22, 23] which can generally be classified as adsorption reaction models and adsorption diffusion models. Because of the complexity involved in the prediction of kinetic parameters, a typical approach consists in fitting experimental data to a series of established models, and selecting the one that provides the best fit. These models lump the mass transfer resistances that can retard the adsorption process (i.e.; external diffusion in the film surrounding the particle, diffusion into the pore system, and surface diffusion) into a single overall mass transfer coefficient.

To assess the suitability of our adsorbents for the separation of CO_2/CH_4 the current contribution investigates the kinetic performance of CS-H_2O and CS-CO_2, two cherry stone-based activated carbons, a detailed characterization of which is provided elsewhere [24] and of a commercially available activated carbon Calgon BPL.. Dynamic adsorption experiments were carried out in a purpose-built lab-scale fixed-bed

unit at different CO_2/CH_4 feed concentrations, at atmospheric pressure and at 30°C. Three kinetic models were used to estimate the rate parameters during the adsorption of CO_2 on these carbons: pseudo-first order, pseudo-second order and Avrami´s fractional order kinetic models. Finally, a fundamental analysis of the mass transfer mechanism controlling CO_2 adsorption on these carbons was performed on the basis of the intra-particle diffusion and the Boyd's film-diffusion models.

2. Materials and methods

2.1. Materials

Two biomass-based activated carbons (CS-H_2O and CS-CO_2) previously prepared in our laboratory from cherry stones, a low-cost biomass residue from the Spanish food industry, have been evaluated as adsorbent materials. Moreover, a commercial activated carbon, Calgon BPL (4x10), has been chosen as a reference for comparison purposes.

CS-H_2O and CS-CO_2 were prepared following a single-step procedure using steam (CS-H_2O) or CO_2 (CS-CO_2) as activating agents. A fully detailed chemical and textural characterization of these carbons has been reported elsewhere [24]. Calgon BPL is a bituminous coal-based carbon that is activated at high temperature with steam. It is therefore a microporous activated carbon with suitable characteristics for CO_2 adsorption. More details about its chemical and textural characteristics can be found elsewhere [20, 25]. Textural parameters of the cherry stone-based carbons and Calgon BPL that may be relevant for discussion are summarized in Table 1.

2.2. Fixed bed adsorption-desorption experiments

In order to evaluate the dynamic performance of the studied adsorbents for separating CO_2 from CO_2/CH_4 gas streams, breakthrough experiments with binary gas mixtures were conducted in a lab-scale fixed-bed reactor with a length of 13.3 cm and an internal diameter of 1.3 cm. A detailed description of the system can be found elsewhere [20, 25].

The column was packed with the activated carbons (4.10, 4.80 and 7.00 g of CS-CO_2, CS-H_2O and BPL, respectively) in order to assess the dynamics of adsorption of CO_2 and CH_4 during the experiments. The breakthrough tests consisted of six consecutive two-step adsorption-desorption cycles in which the adsorbent reached saturation point (maximum adsorption capacity of the adsorbed components) during the adsorption step and was completely regenerated during the desorption step. Simulated biogas streams with different CO_2/CH_4 compositions (30/70, 50/50, and 65/35 vol. %, respectively) were fed into the adsorption unit and the adsorption performance of the samples was evaluated at a temperature of 30 °C and at atmospheric pressure.

In a representative cyclic adsorption-desorption experiment the adsorbent was initially dried by flowing He (50 mL min^{-1} STP) for 60 min at 180 °C and at atmospheric pressure. After the drying step, the bed was cooled down to the adsorption temperature (30 °C) in a preconditioning step of 20 min, during which 50 mL min^{-1} STP of He was made to flow through the system. Adsorption was then begun by feeding the selected CO_2/CH_4 mixture into the pre-conditioned column for 60 min. A total feed gas flow rate of 30 mL min^{-1} STP was kept constant during the adsorption step. The CO_2 and CH_4 concentrations in the gas stream exiting the adsorption column were continuously monitored as a function of time (breakthrough curve) by means of a micro gas chromatograph until the composition approached the inlet gas composition set

point, i.e., until saturation was reached. Afterwards, the adsorbed CO_2 was completely desorbed by raising the temperature of the bed to 180 °C for 60 min at a He flow rate of 50 mL min^{-1} STP. The equilibrium CO_2 adsorption capacity and breakthrough time, t_b, were calculated on the basis of an average of six consecutive cycles. The repeatability of the breakthrough curves was also assessed. The equilibrium adsorption capacities of CO_2 and CH_4 were determined by applying a mass balance to the bed as well as accounting for the gas accumulated in intraparticle voids and dead space. Detailed description can be found in Gil *et al.* [25] and in Appendix A. The breakthrough times were taken at a relative concentration ($C_{i,outlet}/C_{i,feed}$) of 0.05.

Blank experiments were also conducted at 30 °C and at the different CO_2 feed concentrations using a bed packed with glass beads of approximately 3 mm diameter. By means of these experiments it was possible to account for extra-column effects (e.g., gas holdup) during the breakthrough tests. The breakthrough curves of the carbons were also corrected with these blanks to determine the kinetic parameters.

2.3. Kinetic studies

2.3.1. Adsorption rate

Among the properties expected of a good adsorbent, fast adsorption kinetics is one of the most critical since the residence time required for the completion of the adsorption process, adsorption bed size and, consequently, unit capital costs are all intrinsically associated with the rate of adsorption [26, 27]. Most kinetic studies are directed at predicting the rate-limiting step and obtaining a conceptual understanding of the mechanism associated with the adsorption [28]. Among the existing empirical kinetic models, we have considered two of the most extensively applied, namely,

Lagergen´s pseudo-first and pseudo-second order kinetic models. In addition, a fractional order kinetic model based on Avrami´s kinetic model of particle nucleation was also evaluated [29]. It is worth noting that this model has already been applied to predict the adsorption kinetics of CO_2 on amine-functionalized adsorbents [30], and is therefore relevant to our research.

In these models, all the mass transfer resistances to adsorption such as external diffusion, pore diffusion and surface adhesion are lumped together [31]. These models are based on kinetic and diffusion observations at laboratory scale and have been strategically selected since all of them have been identified as suitable for describing the performance of fixed-bed adsorbers [32].

2.3.1.1. Pseudo-first order model

The earliest work reporting a kinetic study was carried out by Lagergren in 1898 [33]. The model which is often applied to liquid phase adsorption is represented by Equation 1:

$$dq_t/dt = k_f(q_e - q_t) \qquad \text{Equation 1}$$

where q_e and q_t (mol kg^{-1}) represent the amount of CO_2 adsorbed at equilibrium and at a given time, respectively and k_f (min^{-1}) is the first order rate constant. With the boundary conditions of t=0, q_t=0 and t=∞, q_t=q_e, Equation 1 can be expressed as follows:

$$q_t = q_e\left(1 - \exp\left(-k_f t\right)\right) \qquad \text{Equation 2}$$

The pseudo-first order model represents a reversible interaction between adsorbent and adsorbate which is suitable for predicting the physical adsorption of CO_2 on solid sorbents [27, 34].

2.3.1.2. Pseudo-second order model

Apart from the pseudo-first-order, the pseudo-second-order model is also often encountered in the literature [23]. The mathematical form of the pseudo-second order equation was first proposed by Blanchard et al. to describe the kinetics of heavy metal removal by natural zeolites [35].

The model can be expressed as:

$$dq_t/dt = k_s(q_e - q_t)^2 \qquad \text{Equation 3}$$

where, k_s (kg mol^{-1} min^{-1}) is the second order kinetic constant. With the boundary conditions of t=0, q_t=0 and t=∞, q_t=q_e, the adsorption capacity at a given time can be expressed as follows:

$$q_t = \frac{q_e^2 k_s t}{1 + q_e k_s t} \qquad \text{Equation 4}$$

The pseudo-second-order model assumes that the interaction between adsorbent and adsorbate is caused by the strong binding of gas molecules to the surface of the adsorbent and has been found suitable for predicting CO_2 sorption behavior based on chemical interactions [36]. This model is also useful for describing solids diffusion rate controlled processes that cannot be properly described by the pseudo-first order model.

2.3.1.3. Avrami´s fractional model

Avrami´s fractional order kinetic model was originally developed to simulate phase transition and crystal growth of materials [29]. The general form of the model is written as follows:

$$dq_t/dt = k_A^{n_A} t^{n_A - 1}(q_e - q_t) \qquad \text{Equation 5}$$

where k_A is the Avrami kinetic constant, and n_A is the Avrami exponent reflecting mechanism changes that may take place during the adsorption process [37, 38]. It also represents the dimensionality of growth of adsoption sites: n_A = 2 for one-dimensional

growth, n_A = 3 for two-dimensional growth, and n_A = 4 for three-dimensional growth [39]. In the case of homogeneous adsorption in which the probability of adsorption occurring is equal for any region for a given time interval, n_A = 1 [40, 41]. An Avrami exponent of exactly 2 indicates perfect one-dimensional growth for adsorption sites which are forming continuously and at a constant rate [39]. The integrated form of Equation 5 is:

$$q_t = q_e\left(1 - exp(-(k_A t)^{n_A})\right) \qquad \text{Equation 6}$$

2.3.1.4. Validation of the kinetic model

To quantitatively evaluate the goodness of fit of the three kinetic models two different error functions, the nonlinear coefficient of determination (R^2) and the residual sum of squares between the experimental mass uptake and that given by the model (Δq), were evaluated. The coefficient of determination, which determines how well the data points fit the model, was calculated as follows [30]:

$$R^2 = 1 - \left(\frac{\sum_{i=1}^{n}\left(q_{t(exp)} - q_{t(model)}\right)^2}{\sum_{i=1}^{n}\left(q_{t(exp)} - \overline{q_{t(exp)}}\right)^2}\right)\left(\frac{n-1}{n-p}\right) \qquad \text{Equation 7}$$

The residual sum of squares, which reflects the deviation between the experimental results and the values predicted by the kinetic models, can be calculated using the following equation:

$$\Delta q(\%) = \sqrt{\frac{\sum_{i=1}^{n}\left(q_{t(\exp)} - q_{t(model)}\right)_i^2}{n-1}}\ \text{x}\ 100 \qquad \text{Equation 8}$$

where the subscripts *"exp"* and *"model"* refer to the measured and model predicted values of the amount adsorbed, respectively; $\overline{q_{t(exp)}}$ is the average value of the experimental data; *n* represents the number of experimental data points fitted for each

sample (from the beginning of the mass uptake up to equilibrium (q/q_e=1)) and p is the number of parameters of the model [30]. Fitting of the models to the experimental data was conducted by means of the Solver Excel tool (Microsoft Office Excel 2010). Values of R^2 close to 1 and a small error function indicate that the model is able to successfully describe the kinetics of the adsorption process.

2.3.2. Adsorption mechanism

The kinetic models described above are convenient for predicting the adsorption behavior of CS-H_2O, CS-CO_2, and Calgon BPL. However, because all the adsorption resistances are lumped together, it is difficult to distinguish the rate-limiting step occurring during the adsorption stages. For porous sorbents such as activated carbons, diffusion effects may be quite important and so the physical meaning of the evaluated rate constant must be determined in order to be able to know the mass transfer mechanism involved [42, 43]. Most commonly, the rate of adsorption is controlled by film diffusion or intra-particle diffusion or both [21, 44, 45].

2.3.2.1. Intra-particle diffusion model

Weber and Morris [46] postulated the intra-particle diffusion model based on Fick´s second law, represented by Equation 9. This model can be used to identify consecutive stages of mass transfer during the adsorption process.

$$q_t = k_{id} t^{1/2} + C \qquad \text{Equation 9}$$

where q_t is the amount adsorbed at any particular time (mol kg^{-1}), k_{id} is the intra-particle diffusion rate constant (mol kg^{-1} $min^{-1/2}$) and C (mol kg^{-1}) refers to the thickness of the boundary layer. According to the Weber-Morris model the plot of q_t *versus* $t^{1/2}$ should give a straight line if diffusion plays a role in the rate of adsorption and this line should pass through the origin if intra-particle diffusion is the sole rate-controlling step.

Nevertheless, it is common to see multi-linearity on the q_t - $t^{1/2}$ plot, which indicates that the adsorption mechanism consists of different stages. Most frequently, three steps in the intra-particle diffusion model can be identified, the first one corresponding to the external diffusion adsorption or boundary layer diffusion, the second one to the gradual stage of adsorption (i.e., intra-particle diffusion, strictly speaking) and the third one to the final equilibrium stage [27]. However, it is generally accepted that the third step is very rapid and does not represent the rate-determining step [47]. In general, the slope of the line in each stage is called the rate parameter $k_{id,i}$ (where i stands for the stage number) and the lowest slope corresponds to the rate-controlling step [27].

2.3.2.2. Boyd´s film-diffusion model

Boyd's model was originally proposed for intra-particle diffusion in a spherical particle, although it is better known as Boyd's film-diffusion model. Given that the CO_2 molecule has to diffuse through the gas film before being adsorbed, the film-diffusion model may be useful for distinguishing whether this external mass transfer resistance is the rate-limiting step. Moreover, whenever two adsorbates are present in the gas mixture, there is the possibility of external resistance to mass transfer.

Boyd´s film-diffusion model assumes that the gas film surrounding the adsorbent particle is the main resistance to adsorption of the adsorbate [48]. This model is expressed as follows:

$$F = 1 - \frac{6}{\pi^2}\sum_{n=1}^{\infty}\frac{1}{n^2}exp(-n^2Bt) \qquad \text{Equation 10}$$

where F is the fractional adsorption capacity at a given time ($F=q_t/q_e$). Bt is a mathematical function of F such that:

For $F > 0.85$, $Bt = f(F) = -0.4977 - ln(1 - F)$ Equation 11

For $F < 0.85$, $Bt = f\ (F) = \left(\sqrt{\pi} - \sqrt{\pi - \left(\frac{\pi^2 F}{3}\right)}\right)^2$ Equation 12

This model can be used to predict the mechanism involved in the adsorption process through the plot of *Bt* against time *t*. If the plot gives a straight line that passes through the origin, the adsorption rate will be controlled by intra-particle diffusion. However, if the plot is not a straight line or does not pass through the origin, it can be inferred that adsorption is *also* influenced by another mass transfer mechanism: film diffusion [49, 50].

3. Results and discussion

3.1. Effect of feed composition

Biogas, which is typically generated at atmospheric pressure, mainly comprises CH_4 and CO_2. The molar fraction of CO_2 in biogas may range from 0.30 to 0.65 depending on its source. The content of other contaminants such as H_2S, O_2, H_2, sulfur, etc., in the water-saturated mixture is below 4% and highly dependent on the source [51, 52]. Since the target gas stream from which CO_2 has to be removed can have a variable CO_2 content, the effect of the feed composition on the separation of CO_2/CH_4 needs to be investigated. We therefore evaluated three binary CO_2/CH_4 gas streams with the following compositions in the present study: 30/70, 50/50 and 65/35 vol.% CO_2/CH_4

Figure 1 displays the breakthrough profiles of CO_2 and CH_4 at 30 ˚C and at atmospheric pressure for the tested activated carbons as a function of the feed composition.

In general, three phases can be identified in the breakthrough curves: i) the breakthrough phase, where the weakest adsorbate quickly breaks through the fixed-bed

column; ii) the competition phase, where CH_4 exhibits a so-called roll-up or roll-over due to the preferential adsorption of CO_2 over CH_4. At this point, the molar flow rate of CH_4 in the effluent is temporarily higher than that fed to the adsorption bed. The CH_4 once adsorbed is displaced by CO_2, whose concentration front advances more slowly through the column than that of CH_4; and finally, iii) the saturation phase, where the adsorbents are completely saturated with adsorbate that can no longer be adsorbed [53]. The amplitude of the roll-up is a measure of the competition between CO_2 and CH_4 for adsorption sites: it is high when a large amount of CH_4 is rapidly replaced by the incoming CO_2. It is observed that at higher CO_2 partial pressures in the feed the height of the roll-up increases but it becomes narrower [20].

The time elapsed between the CH_4 and the CO_2 breakthrough is indicative of the separating capacity of the solids bed: the greater the difference in breakthrough times between both adsorbates, the greater the effectiveness of the separation. Visual inspection of the curves in Figure 1 shows that the quality of separation decreases in the order 30/70 > 50/50 > 65/35 vol.% CO_2/CH_4.

Figure 2 compares the behavior of the different activated carbons at each CO_2 partial pressure tested is compared

According to Figure 2, Calgon BPL shows longer breakthrough times of CO_2 and CH_4 for feed compositions where CO_2 accounts for more than 50 vol.%. However, when the CO_2 concentration in the feed is 30 vol.% (Fig. 2a), CS-H_2O gives a slightly longer breakthrough time for CO_2 than the other carbon materials.

If the shapes of the CO_2 breakthrough curves are analyzed in more detail, it is observed that Calgon BPL displays a more distended mass transfer zone (between the breakthrough point and saturation) than the biomass-based activated carbons in the

whole range of CO_2 partial pressures tested. Therefore, mass transfer of CO_2 into the pores of CS-CO_2 and CS-H_2O may be more favored than the commercial activated carbon. In other words, the data reveal fast kinetics for the adsorption of CO_2 on the cherry stone- based activated carbons. In the case of CH_4, only very small differences are observed between the three carbons evaluated indicating that the kinetics of CH_4 adsorption may not be particularly relevant for the separation of CO_2/CH_4.

The CO_2 and CH_4 adsorption capacities of the three carbon adsorbents at the feed compositions tested are presented in Table 2. These values stand for the average CO_2 and CH_4 uptakes over the six consecutive cycles conducted in each experiment.

As one might expect the adsorption of CO_2 and CH_4 is enhanced with increasing CO_2 and CH_4 concentrations in the feed. For instance, with the increase in CO_2 concentration from 30 to 65 vol.%, CO_2 adsorption on CS-H_2O doubles and reaches 2.12 mol CO_2 kg^{-1}. A similar behavior is observed for all the carbon adsorbents. This is certainly related to the enhancement of the concentration gradient that drives the adsorption process, leading an increase in mass transfer.

3.2. Apparent kinetic model

3.2.1. Comparison of kinetic models

Throughout this section we will analyze the kinetics of CO_2 adsorption associated to CO_2/CH_4 separation by means of adsorption on CS-CO_2, CS-H_2O and Calgon BPL. In the previous section it was suggested that the kinetics of CH_4 adsorption might not play a significant role in this specific CO_2/CH_4 separation.

Three kinetic models were considered: pseudo-first order, pseudo-second order and Avrami´s fractional models. Theoretically, the adsorption of CO_2 on the carbons

evaluated could be described with either one of these three models. However, not all models may be equally suitable for this adsorption process.

Figure 3 presents the evolution with time of the amounts of CO_2 adsorbed on the three carbons during the breakthrough experiments at 30˚C, at atmospheric pressure and for different feed compositions. The points represent the experimental values and the dashed lines the amounts predicted by fitting the experimental data to the kinetic models. Time $t = 0$ on these curves was selected as the inflection point ($dq_t/dt \neq 0$) of the experimental CO_2 breakthrough curves (see Figures 1 and 2).

The values of the kinetic parameters calculated for each model and the corresponding correlation coefficients (R^2) and associated errors (Δq (%)) are listed in Table 3.

It can be seen that the pseudo-first and pseudo-second order kinetic models have certain limitations for predicting CO_2 adsorption on CS-H_2O, CS-CO_2, and Calgon BPL. For instance, the pseudo-first order model overestimates the uptake of CO_2 in the initial stages of adsorption and underestimates the uptake when approaching the equilibrium. Nevertheless, during the final stages of adsorption the pseudo-first order prediction closely follows the trends of the experimental data and the equilibrium CO_2 adsorption capacities are in good agreement with the experimental values. On the other hand, the pseudo-second order model overestimates CO_2 uptake in the initial stages and underestimates the uptake in the final stages since it predicts much lower equilibrium adsorption capacities than the experimental values. A comparison of the values of R^2 and Δq (%) tabulated in Table 3, reveals that the pseudo-second order model gives the worst fitting of the three models: the R^2 values fall within the 0.680-0.915 range and those of Δq (%) between 10 and 38%. As already mentioned in section 2.3.1, the

pseudo-first order model might accurately represent reversible adsorption between the gas and the solid surface as equilibrium is established, while the pseudo-second order is based on the assumption that a strong adsorbate-adsorbent interaction is the rate-controlling step. Consequently, it can be concluded that CO_2 adsorption on CS-H_2O, CS-CO_2 and Calgon BPL does not strictly respond to any of these two mechanisms and follows an intermediate path.

As can be seen in Table 3, Avrami's fractional order model suitably fits the experimental data over the range of feed composition considered, presenting the lowest error function values (maximum Δq of *4.7%)* and values of R^2 close to unity. Therefore, compared with the pseudo-first and pseudo-second order kinetic models, the Avrami equation seems the most accurate approach for describing CO_2 adsorption kinetics on the carbon adsorbents studied. The excellent quality of the fit of the Avrami model to the experimental data at low and high surface coverage is most likely associated with its ability to account for complex reaction pathways [29, 34, 54]. A further advantage of Avrami´s equation is that the kinetic constant is independent of the initial concentration of the adsorbate [55]. Serna-Guerrero et al. [34] also found that the pseudo-first and pseudo-second order kinetic models showed certain limitations for describing CO_2 adsorption on amine-functionalized mesoporous silica and reported that the best kinetic model fit was provided by Avrami´s equation. This model has already been successfully employed to explain kinetic processes on a wide range of adsorbents and adsorbates [38, 54, 56].

For these reasons we chose Avrami's model parameters for a more detailed analysis of the CO_2 adsorption mechanism on CS-CO_2, CS-H_2O and Calgon BPL.

3.2.2. Analysis of kinetic model parameters

The values of the kinetic parameters depicted in Table 3 indicate that for each carbon adsorbent, the adsorption rate constant k_A increases with an increase in the CO_2 concentration. The increase in the mass transfer coefficient with the rise in the concentration of CO_2 in the feed is reflected in the significantly steeper concentration profiles (depicted in Figures 1-3). The trend observed agrees well with the data reported in the literature [57].

As we mentioned in section 2.3.1.3 the Avrami exponent (n_A) is a fractional number that accounts for possible changes of the adsorption mechanism during the adsorption process. Instead of following a single integer-kinetic order the mechanism of adsorption might follow multiple kinetic orders that change during the contact of the adsorbate with the adsorbent. Therefore n_A is the result of multiple kinetic orders occurring in the adsorption process. A progressive increase in the values of n_A with feed concentration was observed for the carbon adsorbents. The increase in the Avrami exponent with the CO_2 feed concentration indicates that the adsorption of CO_2 seems to have more contact time dependence at elevated concentrations. The Avrami exponent, n_A, as determined from our experimental data lies in the 1.529 - 2.334 range, confirming the co-existence of different adsorption mechanisms [54].

Furthermore, consistent with the previous observation that our biomass-based activated carbons showed a more enhanced kinetic behavior than the commercial activated carbon (see Figure 4), the calculated values of the global mass transfer coefficient (k_A) for CO_2 adsorption on CS-H_2O and CS-CO_2 in the fixed bed are higher than those of Calgon BPL. As shown in Table 3, the values of k_A are 0.441 and 0.410 min^{-1} for CS-H_2O and CS-CO_2, respectively, when feeding CO_2 at 30 vol.% whereas for

Calgon BPL the limit is 0.267 min^{-1}. The same pattern was observed for the other two feed concentrations tested in this work.

Moreover, the calculated values of the kinetic rate constants for the biomass based activated carbons (0.2 $min^{-1} < k_A < 0.6\ min^{-1}$) are consistent with values reported in the literature for activated carbons [58].

The estimated values for the parameter n_A in the Avrami model for the commercial activated carbon were also found to be lower than those of the biomass-based activated carbons. As previously mentioned, this parameter is related to changes in the mechanism occurring during the adsorption process so the difference between the biomass-based carbons and Calgon BPL may be indicative of different adsorption pathways.

3.3. Rate-limiting adsorption stage

For porous adsorbents, such as activated carbons, diffusion-based effects may be very important and so the physical significance of the evaluated rate constants needs to be properly ascertained to gain an accurate insight into mass transfer mechanisms involved.

The possibility of intra-particle diffusion resistance controlling the adsorption of CO_2 on the evaluated activated carbons was explored using Equation 9. Figure 4 shows the intra-particle diffusion plots at the CO_2 feed concentrations tested for CS-H_2O, CS-CO_2 and Calgon BPL. The intra-particle diffusion constant, k_{id} (mol kg^{-1} $min^{-1/2}$), can be estimated from the slope of the plot of q_t (mol kg^{-1}) versus the square root of time.

When intra-particle diffusion occurs, the plot q_t versus $t^{1/2}$ is linear and if it passes through the origin, then the rate limiting process is only due to intra-particle

diffusion [59]. Figure 4 shows the intra-particle diffusion plot at different CO_2 partial pressures for each adsorbent tested in this work.

It is clearly observed in Figure 4 that the plots are not linear over the whole time range. They show multi-linearity for CO_2 adsorption on CS-H_2O, CS-CO_2 and Calgon BPL. This means that intra-particle diffusion model is not the sole rate limiting mechanism in the adsorption process: more than one single kinetic stage is involved in the process of CO_2 adsorption on these carbons and each stage can be attributed to each linear section of the plot. Two main stages can be identified in the plots, suggesting that the adsorption of CO_2 concurrently occurs by diffusion of CO_2 through the external surface of the adsorbent (first linear region) and by intra-particle diffusion (second linear region). However, at the highest CO_2 partial pressure (65 vol.% CO_2) only one linear region is observed for the biomass-based activated carbons (Figures 6a and 6b) but it does not pass through the origin. This might suggest that the intraparticle diffusion model is applicable but that it is not the only rate-controlling mechanism.

The values of k_{id} estimated from the slope of each linear region are tabulated in Table 4 and referred to as $k_{id,1}$ and $k_{id,2}$, respectively. The R_i^2-values (with i = 1, 2) obtained from fitting them to each rectilinear plot were found to be close to unity, confirming the applicability of this model.

The values of $k_{id,1}$ are larger than $k_{id,2}$ at any CO_2 partial pressure indicating that film diffusion of CO_2 molecules towards the carbon surfaces was relatively fast [60]. The faster uptake of CO_2 in the first region can be attributed to rapid diffusion of CO_2 to the external surface. When the external surface area is saturated intra-particle diffusion will begin to take place and diffusion to the inner sites, (i.e., macropores, mesopores and micropores) will occur. The lower k_{id} values in the second region, ascribed to intra-

particle diffusion, indicate that this stage occurs at a slower pace thus being more relevant to the overall rate of adsorption [17].

The calculated values of $k_{id,2}$ (mol kg^{-1} min$^{-1/2}$) are greater for the biomass-based activated carbons than for commercial Calgon BPL. In addition, the value of $k_{id,2}$ increases with the increase in inlet CO_2 concentration. These results indicate that intra-particle diffusion proceeds faster in CS-CO_2 and CS-H_2O than in Calgon BPL.

As we demonstrated in our previous study [20], the bed of Calgon BPL shows less total porosity (0.79) than that of the biomass-based adsorbents (0.84 and 0.86 for CS-H_2O and CS-CO_2, respectively). To calculate the total porosity of the bed we took into account the packed bed porosity and the particle porosity [25]. It should also be pointed out that a similar bed height was established in all the breakthrough experiments. Moreover, the particle size of Calgon BPL (2-4.75 mm) is greater than that of the biomass carbons (1-3 mm). Therefore, these two differential features might explain the faster kinetics of CO_2 adsorption on the cherry stone-based carbons.

In order to confirm our interpretations of the intra-particle diffusion model analysis about the rate-controlling step during the adsorption process, the experimental data were further analyzed by applying Boyd's film model represented by Equation 10.

Figure 5 shows the plots of *f(F)* versus time under different CO_2 partial pressures. All the plots exhibit a linear pattern but do not pass through the origin, indicating that the adsorption process is not solely influenced by intra-particle diffusion. This is in good agreement with our results from the intra-particle diffusion model. The values of the kinetic parameter *B* are summarized in the Table 5. They follow the same trend as that observed in the fitting of the intra-particle diffusion model: the rate

constants are higher for the biomass-based activated carbons than for commercial Calgon BPL and they increase with the increase in the inlet CO_2 concentration.

From the above results it can be concluded that two main mechanisms are involved in mass transfer during the overall process of adsorption of CO_2 on CS-H_2O, CS-CO_2 and Calgon BPL in the range of the CO_2 partial pressures evaluated. However, only one mechanism governs the adsorption process at a given time: during the initial stages, film diffusion of CO_2 is the main resistance to mass transfer and controls the adsorption rate; once CO_2 has diffused through the gas film, the network of pores in the adsorbent bed make intra-particle diffusion the rate-limiting step that controls adsorption until equilibrium is attained.

4. Conclusions

This study presents for the first time a kinetic analysis of CO_2 adsorption on biomass-based activated carbon for biogas upgrading.

The kinetics of CO_2 adsorption on CS-H_2O, CS-CO_2 and Calgon BPL were evaluated by means of three adsorption reaction models (pseudo-first order, pseudo-second order, and Avrami´s kinetic models) and two adsorption diffusion models (intra-particle and Boyd's film diffusion). The best fit of the experimental data for all adsorbents over the wide range of feed compositions tested was obtained by applying Avrami´s kinetic model and the adsorption rate constants, k_A, were found to increase with increasing CO_2 concentration. Adsorption diffusion models were applied to identify the CO_2 adsorption mechanism on these carbons. It was found that mass transfer during the adsorption of CO_2 on these carbons proceeds through a diffusion-based process involving film diffusion and intra-particle diffusion. At the initial stage of

adsorption, diffusion through the film is dominant. When the amount of CO_2 in the external film reaches a certain point, intra-particle diffusion takes over.

In addition, the faster kinetics of CO_2 adsorption on the cherry stone- based carbons was confirmed, lending support to our previous conclusions drawn from the equilibrium of adsorption results on the suitability of these biomass-based carbons for CO_2/CH_4 separation.

Acknowledgements

This work has received financial support from the Spanish MINECO (Project ENE2011-23467), co-financed by the European Regional Development Fund (ERDF), and from the Gobierno del Principado de Asturias (PCTI 2013-2017 GRUPIN14-079). N.A-G. also acknowledges a fellowship awarded by the Spanish MINECO (FPI program), and co-financed by the European Social Fund.

Appendix A. Supplementary Content

Methodology to evaluate the CO_2 and CH_4 adsorption capacity from breakthrough experiments

References

[1] S.U. Rege, R.T. Yang, K. Qian, M.A. Buzanowski, Air-prepurification by pressure swing adsorption using single/layered beds, Chemical Engineering Science, 56 (2001) 2745-2759.
[2] M.M. Hassan, D.M. Ruthven, N.S. Raghavan, Air separation by pressure swing adsorption on a carbon molecular sieve, Chemical Engineering Science, 41 (1986) 1333-1343.
[3] A. Malek, S. Farooq, Hydrogen purification from refinery fuel gas by pressure swing adsorption, AIChE Journal, 44 (1998) 1985-1992.
[4] J. Stocker, M. Whysall, C.Q. Miller, "30 years of PSA technology for hydrogen purification", (1998).

[5] F.V.S. Lopes, C.A. Grande, A.E. Rodrigues, Activated carbon for hydrogen purification by pressure swing adsorption: Multicomponent breakthrough curves and PSA performance, Chemical Engineering Science, 66 (2011) 303-317.
[6] S. Sircar, T.C. Golden, Purification of hydrogen by pressure swing adsorption, Separation Science and Technology, 35 (2000) 667-687.
[7] S. García, M.V. Gil, J.J. Pis, F. Rubiera, C. Pevida, Cyclic operation of a fixed-bed pressure and temperature swing process for CO_2 capture: Experimental and statistical analysis, International Journal of Greenhouse Gas Control, 12 (2013) 35-43.
[8] G.D. Pirngruber, D. Leinekugel-le-Cocq, Design of a pressure swing adsorption process for postcombustion CO_2 capture, Industrial & Engineering Chemistry Research, 52 (2013) 5985-5996.
[9] S. Sircar, Pressure swing adsorption, Industrial and Engineering Chemistry Research, 41 (2002) 1389-1392.
[10] S. Sircar, Separation of methane and carbon dioxide gas mixtures by pressure swing adsorption, Separation Science and Technology, 23 (1988) 519-529.
[11] B.C. Bai, S. Cho, H.-R. Yu, K.B. Yi, K.-D. Kim, Y.-S. Lee, Effects of aminated carbon molecular sieves on breakthrough curve behavior in CO_2/CH_4 separation, Journal of Industrial and Engineering Chemistry, 19 (2013) 776-783.
[12] S. Cavenati, C.A. Grande, A.E. Rodrigues, Adsorption equilibrium of methane, carbon dioxide, and nitrogen on zeolite 13X at high pressures, Journal of Chemical and Engineering Data, 49 (2004) 1095-1101.
[13] P.S. Barcia, L. Bastin, E.J. Hurtado, J.A.C. Silva, A.E. Rodrigues, B. Chen, Single and multicomponent sorption of CO_2, CH_4 and N_2 in a microporous metal-organic framework, Separation Science and Technology, 43 (2008) 3494-3521.
[14] V. Goetz, O. Pupier, A. Guillot, Carbon dioxide-methane mixture adsorption on activated carbon, Adsorption, 12 (2006) 55-63.
[15] Q. Wang, J. Luo, Z. Zhong, A. Borgna, CO_2 capture by solid adsorbents and their applications: current status and new trends, Energy & Environmental Science, 4 (2011) 42-55.
[16] Y. Sun, P.A. Webley, Preparation of activated carbons with large specific surface areas from biomass corncob and their adsorption equilibrium for methane, carbon dioxide, nitrogen, and hydrogen, Industrial and Engineering Chemistry Research, 50 (2011) 9286-9294.
[17] N.A. Rashidi, S. Yusup, A. Borhan, L.H. Loong, Experimental and modelling studies of carbon dioxide adsorption by porous biomass derived activated carbon, Clean Technologies and Environmental Policy, 16 (2014) 1353-1361.
[18] A.S. González, M.G. Plaza, F. Rubiera, C. Pevida, Sustainable biomass-based carbon adsorbents for post-combustion CO_2 capture, Chemical Engineering Journal, 230 (2013) 456-465.
[19] N. Álvarez-Gutiérrez, M.V. Gil, F. Rubiera, C. Pevida, Adsorption performance indicators for the CO_2/CH_4 separation: Application to biomass-based activated carbons, Fuel Processing Technology, 142 (2016) 361-369.
[20] N. Álvarez-Gutiérrez, S. García, M.V. Gil, F. Rubiera, C. Pevida, Dynamic Performance of Biomass-Based Carbons for CO_2/CH_4 Separation. Approximation to a Pressure Swing Adsorption Process for Biogas Upgrading, Energy & Fuels, 30 (2016) 5005-5015..

[21] G. Song, X. Zhu, R. Chen, Q. Liao, Y.-D. Ding, L. Chen, An investigation of CO_2 adsorption kinetics on porous magnesium oxide, Chemical Engineering Journal, 283 (2016) 175-183.
[22] H. Qiu, L. Lv, B.-c. Pan, Q.-j. Zhang, W.-m. Zhang, Q.-x. Zhang, Critical review in adsorption kinetic models, Journal of Zhejiang University SCIENCE A, 10 (2009) 716-724.
[23] Y.S. Ho, G. McKay, Pseudo-second order model for sorption processes, Process Biochemistry, 34 (1999) 451-465.
[24] N. Álvarez-Gutiérrez, M.V. Gil, F. Rubiera, C. Pevida, Cherry-stones-based activated carbons as potential adsorbents for CO_2/CH_4 separation: effect of the activation parameters, Greenhouse Gases: Science and Technology, 5 (2015) 812-825.
[25] M.V. Gil, N. Álvarez-Gutiérrez, M. Martínez, F. Rubiera, C. Pevida, A. Morán, Carbon adsorbents for CO_2 capture from bio-hydrogen and biogas streams: Breakthrough adsorption study, Chemical Engineering Journal, 269 (2015) 148-158.
[26] E.R. Monazam, J. Spenik, L.J. Shadle, Fluid bed adsorption of carbon dioxide on immobilized polyethylenimine (PEI): Kinetic analysis and breakthrough behavior, Chemical Engineering Journal, 223 (2013) 795-805.
[27] S. Loganathan, M. Tikmani, S. Edubilli, A. Mishra, A.K. Ghoshal, CO_2 adsorption kinetics on mesoporous silica under wide range of pressure and temperature, Chemical Engineering Journal, 256 (2014) 1-8.
[28] S. Sohn, D. Kim, Modification of Langmuir isotherm in solution systems—definition and utilization of concentration dependent factor, Chemosphere, 58 (2005) 115-123.
[29] E.C.N. Lopes, F.S.C. Dos Anjos, E.F.S. Vieira, A.R. Cestari, An alternative Avrami equation to evaluate kinetic parameters of the interaction of Hg(II) with thin chitosan membranes, Journal of Colloid and Interface Science, 263 (2003) 542-547.
[30] L. Stevens, K. Williams, W.Y. Han, T. Drage, C. Snape, J. Wood, J. Wang, Preparation and CO_2 adsorption of diamine modified montmorillonite via exfoliation grafting route, Chemical Engineering Journal, 215–216 (2013) 699-708.
[31] D.D. Do, H.D. Do, Non-isothermal effects on adsorption kinetics of hydrocarbon mixtures in activated carbon, Separation and Purification Technology, 20 (2000) 49-65.
[32] C.O. Castillo-Araiza, G. Che-Galicia, A. Dutta, G. Guzmán-González, C. Martínez-Vera, R.S. Ruíz-Martínez, Effect of diffusion on the conceptual design of a fixed-bed adsorber, Fuel, 149 (2015) 100-108.
[33] S. Lagergren, Zur Theorie der Sogenannten Adsorption Gelöster Stoffe, Kungliga Svenska Vetenskapsakademiens, Handlingar, 24 (1898) 1-39.
[34] R. Serna-Guerrero, A. Sayari, Modeling adsorption of CO_2 on amine-functionalized mesoporous silica. 2: Kinetics and breakthrough curves, Chemical Engineering Journal, 161 (2010) 182-190.
[35] G. Blanchard, M. Maunaye, G. Martin, Removal of heavy metals from waters by means of natural zeolites, Water Research, 18 (1984) 1501-1507.
[36] J.M. Borah, J. Sarma, S. Mahiuddin, Adsorption comparison at the α-alumina/water interface: 3,4-Dihydroxybenzoic acid vs. catechol, Colloids and Surfaces A: Physicochemical and Engineering Aspects, 387 (2011) 50-56.
[37] E.W. de Menezes, E.C. Lima, B. Royer, F.E. de Souza, B.D. dos Santos, J.R. Gregório, T.M.H. Costa, Y. Gushikem, E.V. Benvenutti, Ionic silica based hybrid material containing the pyridinium group used as an adsorbent for textile dye, Journal of Colloid and Interface Science, 378 (2012) 10-20.

[38] A.R. Cestari, E.F.S. Vieira, J.D.S. Matos, D.S.C. Dos Anjos, Determination of kinetic parameters of Cu(II) interaction with chemically modified thin chitosan membranes, Journal of Colloid and Interface Science, 285 (2005) 288-295.
[39] J.B. Benedict, P. Coppens, Kinetics of the single-crystal to single-crystal two-photon photodimerization of α-trans-cinnamic acid to α-truxillic acid, The Journal of Physical Chemistry A, 113 (2009) 3116-3120.
[40] M. Avrami, Kinetics of phase change. I: General theory, The Journal of Chemical Physics, 7 (1939) 1103-1112.
[41] M. Avrami, Granulation, phase change, and microstructure kinetics of phase change. III, The Journal of Chemical Physics, 9 (1941) 177-184.
[42] I. Tsibranska, E. Hristova, Comparison of different kinetic models for adsorption of heavy metals onto activated carbon from apricot stones, Bulgarian Chemical Communications, 43 (2011) 370-377.
[43] S.I. Garcés-Polo, J. Villarroel-Rocha, K. Sapag, S.A. Korili, A. Gil, A comparative study of CO_2 diffusion from adsorption kinetic measurements on microporous materials at low pressures and temperatures, Chemical Engineering Journal, 302 (2016) 278-286.
[44] L. Ai, M. Li, L. Li, Adsorption of methylene blue from aqueous solution with activated carbon/cobalt ferrite/alginate composite beads: kinetics, isotherms, and thermodynamics, Journal of Chemical & Engineering Data, 56 (2011) 3475-3483.
[45] H. Yu, X. Wang, C. Xu, D.L. Chen, W. Zhu, R. Krishna, Utilizing transient breakthroughs for evaluating the potential of Kureha carbon for CO_2 capture, Chemical Engineering Journal, 269 (2015) 135-147.
[46] W. Weber, J. Morris, Advances in water pollution research: removal of biologically resistant pollutant from waste water by adsorption, in: P. Press (Ed.) International Conference on Water Pollution Syposium, 1962, pp. 231-236.
[47] D. Mohan, K.P. Singh, Single- and multi-component adsorption of cadmium and zinc using activated carbon derived from bagasse—an agricultural waste, Water Research, 36 (2002) 2304-2318.
[48] G.E. Boyd, A.W. Adamson, L.S. Myers, The exchange adsorption of ions from aqueous solutions by organic zeolites. II. Kinetics1, Journal of the American Chemical Society, 69 (1947) 2836-2848.
[49] B.H. Hameed, I.A.W. Tan, A.L. Ahmad, Adsorption isotherm, kinetic modeling and mechanism of 2,4,6-trichlorophenol on coconut husk-based activated carbon, Chemical Engineering Journal, 144 (2008) 235-244.
[50] P. Sharma, M.R. Das, Removal of a cationic dye from aqueous solution using graphene oxide nanosheets: investigation of adsorption parameters, Journal of Chemical & Engineering Data, 58 (2013) 151-158.
[51] W.H. Zhou, J.P. Guo, H.Y. Tan, Upgrading of methane from biogas by pressure swing adsorption, in: Advanced Materials Research, 2011, pp. 268-271.
[52] T. Remy, E. Gobechiya, D. Danaci, S.A. Peter, P. Xiao, L. Van Tendeloo, S. Couck, J. Shang, C.E.A. Kirschhock, R.K. Singh, J.A. Martens, G.V. Baron, P.A. Webley, J.F.M. Denayer, Biogas upgrading through kinetic separation of carbon dioxide and methane over Rb- and Cs-ZK-5 zeolites, RSC Advances, 4 (2014) 62511-62524.
[53] L. Hauchhum, P. Mahanta, J. De Wilde, Capture of CO_2 from flue gas onto coconut fibre-based activated carbon and zeolites in a fixed bed, Transport in Porous Media, 110 (2015) 503-519.
[54] A.R. Cestari, E.F.S. Vieira, G.S. Vieira, L.E. Almeida, The removal of anionic dyes from aqueous solutions in the presence of anionic surfactant using

aminopropylsilica-A kinetic study, Journal of Hazardous Materials, 138 (2006) 133-141.
[55] B. Royer, N.F. Cardoso, E.C. Lima, J.C.P. Vaghetti, N.M. Simon, T. Calvete, R.C. Veses, Applications of Brazilian pine-fruit shell in natural and carbonized forms as adsorbents to removal of methylene blue from aqueous solutions-Kinetic and equilibrium study, Journal of Hazardous Materials, 164 (2009) 1213-1222.
[56] C.E. Zubieta, P.V. Messina, C. Luengo, M. Dennehy, O. Pieroni, P.C. Schulz, Reactive dyes remotion by porous TiO_2-chitosan materials, Journal of Hazardous Materials, 152 (2008) 765-777.
[57] Q. Liu, J. Shi, S. Zheng, M. Tao, Y. He, Y. Shi, Kinetics studies of CO_2 adsorption/desorption on amine-functionalized multiwalled carbon nanotubes, Industrial and Engineering Chemistry Research, 53 (2014) 11677-11683.
[58] M.S. Shafeeyan, W.M.A.W. Daud, A. Shamiri, N. Aghamohammadi, Modeling of carbon dioxide adsorption onto ammonia-modified activated carbon: kinetic analysis and breakthrough behavior, Energy and Fuels, 29 (2015) 6565-6577.
[59] C.-H. Wu, Adsorption of reactive dye onto carbon nanotubes: Equilibrium, kinetics and thermodynamics, Journal of Hazardous Materials, 144 (2007) 93-100.
[60] M.F. Elkady, A.M. Ibrahim, M.M.A. El-Latif, Assessment of the adsorption kinetics, equilibrium and thermodynamic for the potential removal of reactive red dye using eggshell biocomposite beads, Desalination, 278 (2011) 412-423.

Figure captions

Figure 1. CO_2 (solid lines) and CH_4 (dashed lines) breakthrough curves for CS-H_2O (a), CS-CO_2 (b), and Calgon BPL (c) with 30/70 vol.% CO_2/CH_4 (blue color), 50/50 vol.% CO_2/CH_4 (red color), and 65/35 vol.% CO_2/CH_4 (green color).

Figure 2. CO_2 (solid lines) and CH_4 (dashed lines) breakthrough curves for CS-H_2O (green color), CS-CO_2 (red color), and Calgon BPL (blue color) with 30/70 vol.% CO_2/CH_4 (a), 50/50 vol.% CO_2/CH_4 (b), and 65/35 vol.% CO_2/CH_4 (c).

Figure 3. Evolved amounts of CO_2 adsorbed. Comparison of predicted and experimental CO_2 uptakes on CS-H_2O (a), CS-CO_2 (b), and Calgon BPL (c) at 30˚C and at atmospheric pressure as a function of the feed concentration.

Figure 4. Amount of CO_2 adsorbed versus $t^{1/2}$ (intra-particle diffusion model plot): CS-H_2O (a), CS-CO_2 (b), and Calgon BPL (c). Colors refer to CO_2 partial pressures in the feed stream: 30/70 vol.% CO_2/CH_4 (blue color), 50/50 vol.% CO_2/CH_4 (red color), and 65/35 vol.% CO_2/CH_4 (green color).

Figure 5. Plots of Boyd´s film model for CO_2 adsorption on CS-H_2O (a), CS-CO_2 (b), and Calgon BPL (c) at different CO_2 partial pressures at 30˚C and atmospheric pressure. Colors refer to CO_2 partial pressures in the feed stream: 30/70 vol.% CO_2/CH_4 (blue color), 50/50 vol.% CO_2/CH_4 (red color), and 65/35 vol.% CO_2/CH_4 (green color).

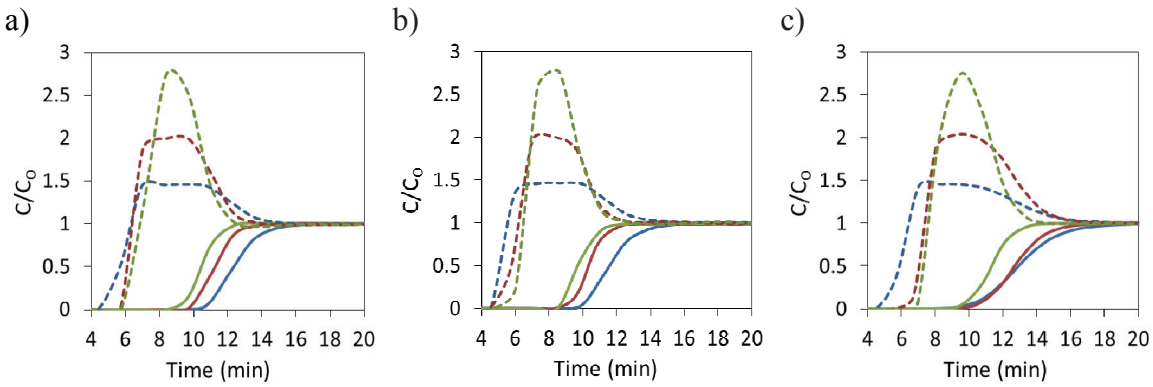

Figure 1.

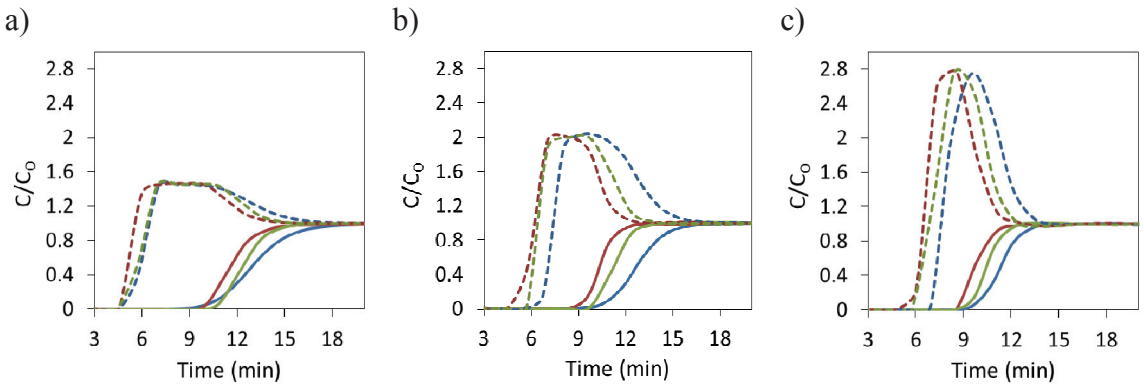

Figure 2.

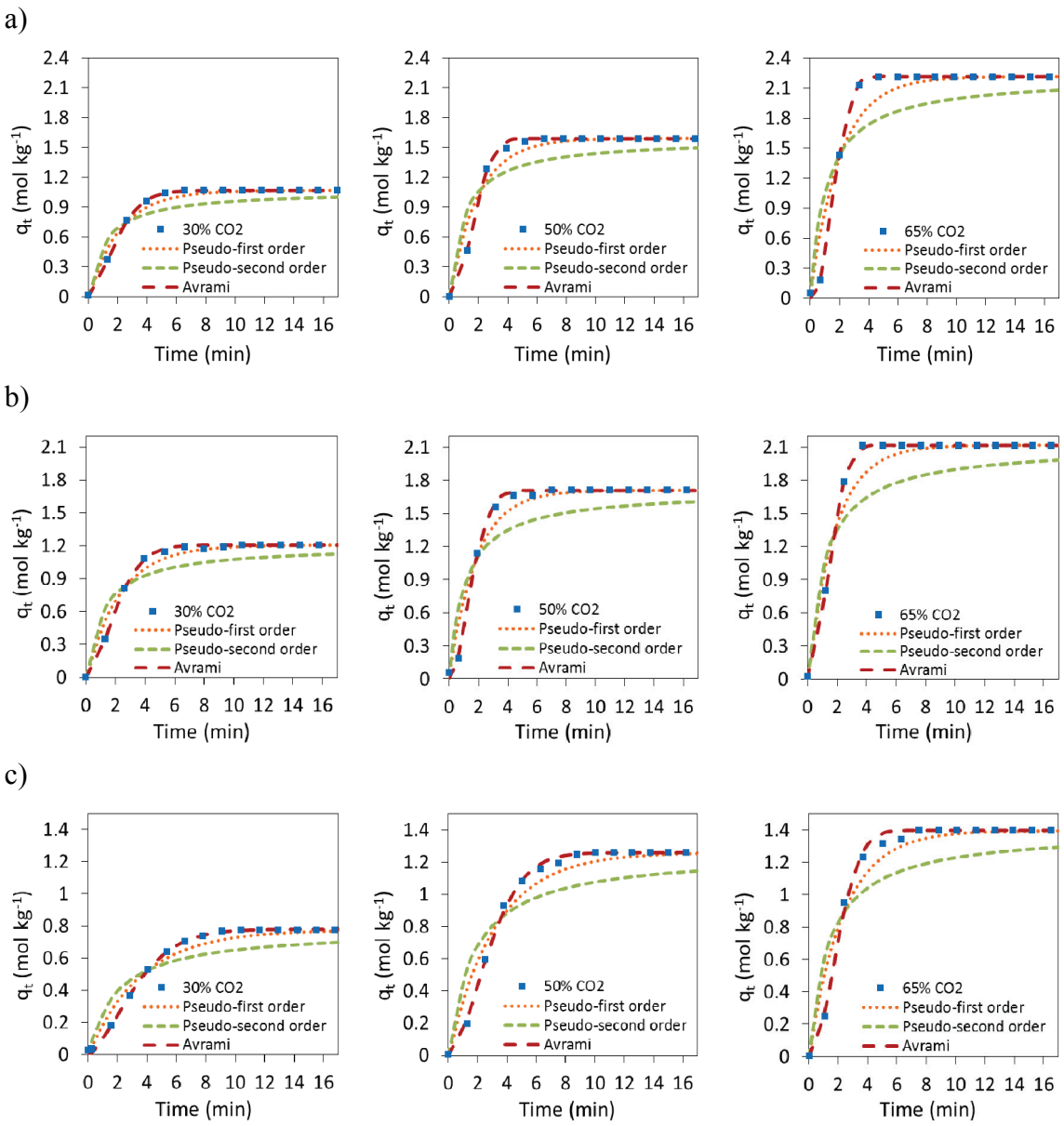
a)
b)
c)
q_t (mol kg^{-1})
Time (min)
30% CO2
50% CO2
65% CO2
Pseudo-first order
Pseudo-second order
Avrami

Figure 3.

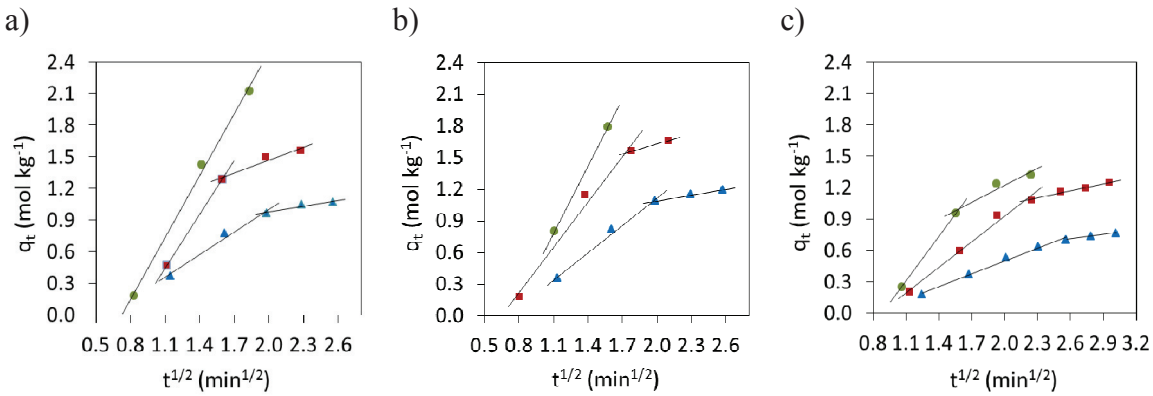
a)
b)
c)
2.4
2.1
1.8
1.5
1.2
0.9
0.6
0.3
0.0
q_t (mol kg^{-1})
c_t (mol kg^{-1})
0.5 0.8 1.1 1.4 1.7 2.0 2.3 2.6
0.8 1.1 1.4 1.7 2.0 2.3 2.6 2.9 3.2
$t^{1/2}$ (min$^{1/2}$)

Figure 4.

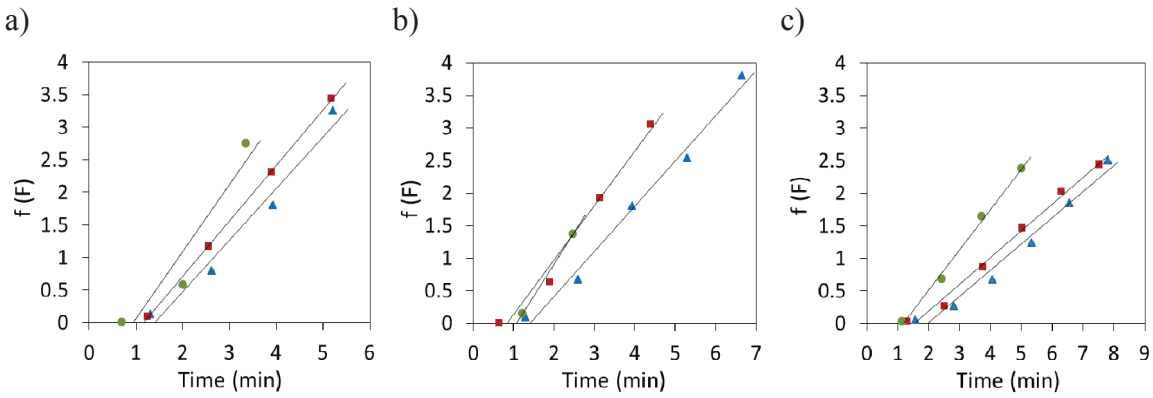

Figure 5.

Table 1. Textural characteristics of the activated carbons.

Sample	S_{BET} (m^2 g^{-1})	V_p (cm^3 g^{-1})	$W_{0,N2}$ (cm^3 g^{-1})	$W_{0,CO2}$ (cm^3 g^{-1})
CS-CO_2	1045	0.48	0.40	0.35
CS-H_2O	998	0.53	0.38	0.33
Calgon BPL	1129	0.50	0.46	0.22

S_{BET}: BET surface area; V_p: total pore volume; $W_{0,N2}$: micropore volume; $W_{0,CO2}$: narrow micropore volume

Table 2. Adsorbed amounts of CO_2 and CH_4 on CS-CO_2, CS-H_2O, and Calgon BPL for the CO_2/CH_4 separations at 30°C and at atmospheric pressure.

Adsorbent	CO_2 adsorption capacity (mol kg^{-1})	CH_4 adsorption capacity (mol kg^{-1})
	30% CO_2 - 70% CH_4	
CS-H_2O	1.04	0.68
CS-CO_2	1.18	0.71
Calgon BPL	0.73	0.42
	50% CO_2 - 50% CH_4	
CS-H_2O	1.49	0.37
CS-CO_2	1.63	0.47
Calgon BPL	1.17	0.32
	65% CO_2 - 35% CH_4	
CS-H_2O	2.12	0.31
CS-CO_2	1.98	0.39
Calgon BPL	1.33	0.23

Table 3. Kinetic model parameters for adsorption on CS-CO_2, CS-H_2O and Calgon BPL at 30°C and at atmospheric pressure for different CO_2 concentrations in the feed.

CO_2 (vol.%)	Sample	Pseudo-first order			Pseudo-second order			Avrami			
		k_f	Δq	R^2	k_s	Δq	R^2	k_A	n_A	Δq	R^2
30	CS-H_2O	0.465	7.622	0.960	0.829	14.737	0.849	0.441	1.556	0.444	1.000
	CS-CO_2	0.433	9.243	0.976	0.703	17.579	0.915	0.410	1.643	1.333	0.999
	BPL	0.280	5.239	0.966	0.660	10.334	0.869	0.267	1.529	0.833	0.999
50	CS-H_2O	0.511	17.034	0.919	0.618	27.172	0.795	0.489	2.049	3.621	0.995
	CS-CO_2	0.548	18.980	0.920	0.547	30.738	0.790	0.540	1.894	3.840	0.995
	BPL	0.314	10.649	0.943	0.464	19.208	0.814	0.301	1.663	2.847	0.995
65	CS-H_2O	0.499	32.872	0.843	0.408	37.732	0.680	0.505	2.334	0.443	1.000
	CS-CO_2	0.542	22.768	0.871	0.412	31.959	0.746	0.556	1.957	0.000	1.000
	BPL	0.425	16.069	0.902	0.521	24.484	0.773	0.421	1.929	4.725	0.987

k_f [=] min^{-1}, k_s [=] kg mol^{-1} min^{-1}, k_A [=] min^{-1}, Δq [=] %

Table 4. Parameters from linear fitting of the intra-particle diffusion model.

CO_2 (vol %)	Sample	$k_{id,1}$	R_1^2	$k_{id,2}$	R_2^2
30	CS-H_2O	0.713	0.984	0.188	0.929
	CS-CO_2	0.865	0.993	0.178	0.993
	BPL	0.410	0.991	0.140	0.996
50	CS-H_2O	1.696	1	0.405	0.950
	CS-CO_2	1.437	0.985	0.319	1
	BPL	0.816	0.986	0.224	0.986
65	CS-H_2O	1.958*	0.996*	—	—
	CS-CO_2	2.132*	1*	—	—
	BPL	1.413	1	0.544	0.942

$k_{id,1}$, $k_{id,2}$ [=] mol kg^{-1} $min^{-1/2}$, *k_{id} and R^2 for the single rectilinear plot.

Table 5. Kinetic parameter *B* estimated from the fitting of Boyd´s film-diffusion model.

CO_2 (vol %)	Sample	*B* (min^{-1})	R^2
30	CS-H_2O	0.793	0.971
	CS-CO_2	0.691	0.988
	BPL	0.402	0.974
50	CS-H_2O	0.850	0.999
	CS-CO_2	0.833	0.983
	BPL	0.410	0.991
65	CS-H_2O	1.032	0.902
	CS-CO_2	0.977	1
	BPL	0.618	0.974